Distributed Control of a Grid-connected PV-battery System for Constant Power Generation

Parviz Talebi[1] and Mohammad Hejri[1,*]

[1] *Department of Electrical Engineering, Sahand University of Technology, Tabriz, Iran*
**Corresponding author: hejri@sut.ac.ir*

Manuscript received 29 December, 2018; Revised 1 March, 2019; accepted 4 March, 2019. Paper no. JEMT -1812-1145.

The classical power supervisory controllers in microgrids generally have a centralized structure to determine the power reference signals of their units. However, by increasing the number and variety of energy storage or other generation units in these systems, the algorithmic complexity of centralized power management controllers increases and their reliability decreases by the addition of new units or outgoing the existing ones. Furthermore, their implementation in outer layers of a hierarchical control system, generally requires a switching between local controllers in the inner layers, with the requirement of bumpless switching to prevent the creation of transient states. To solve these problems, this paper presents a distributed power management system to control the amount of power produced by a microgrid consisting of photovoltaic (PV) arrays and battery storage system to provide the constant power requirement of the grid. Of the merits of the proposed method, one can mention its simplicity, plug-and-play feature, modularity, more reliability, and no requirement to any switching operations in the local controllers of the PV-battery system. Moreover, in the proposed method, the operating point on the PV array power-voltage (P-V) curve can easily be shifted to the left or right-hand side of the maximum power point (MPP), creating more controllability and flexibility for the constant power generation of the entire system. The satisfactory operation of the proposed distributed control algorithm is verified through the numerical simulations of a 100 kW PV-battery system in a wide range of operating points and for critical operation modes such as fully-charged and fully-discharged batteries.

Keywords: *PV-battery system, Grid-connected, Constant power, Centralized control, Distributed control, Microgrid.*

http://dx.doi.org/10.22109/jemt.2019.164589.1145

1. Introduction

Nowadays, renewable energy sources, especially photovoltaic (PV) energy, play a vital role in replacing of traditional fossil fuels. By 2050, the total installed PV capacity is estimated at 3000 GW. This installed capacity has the energy generation capability of 4500 TWh per year, which is about 11% of the total electricity production. In addition to reducing the CO2 emissions by 2.3 giga tone per year, this installed capacity will have many benefits in terms of sustainable energy production and development of various industrial sectors [1]. By reducing production costs, improving the efficiency and progress of PV technology, a large number of these types of power generation units are connecting into the grid that their better integration, power management, and energy storage are of strategic research areas [2].

The power produced by PV systems with high penetration levels is constantly changing due to the climatic changes in the form of variations in the temperature and radiation levels. These power variations disturb the balance between production and consumption, creating problems in terms of voltage and frequency stability, and power quality quantities on the network to which they are connected. From voltage fluctuation point of view, this problem is more evident in distribution systems where the X/R ratio is small, and the reactive power control is not efficient enough [3]. In this regard, to achieve the smooth operation of power systems, the active power fluctuations generated by these sources should be limited to a certain standard degree. One of the solutions is to use energy storage resources, such as batteries, and develop suitable power management algorithms for these systems [4]. In this regard, many studies are going on to minimize the side effects resulting from the variable output power of PV systems and maintain their power profile as constant as possible [5]. In [6], a comprehensive control and power management system is proposed for PV-battery-based hybrid microgrids with both AC and DC buses, and for both grid-connected and islanded modes. The proposed power management algorithm in this work has a centralized structure, which means that the reference power signals for the various units in the grid are determined by a single algorithm. In this paper, two different controllers are used to operate the PV array at the maximum power point (MPP) and below it, which depending on the conditions and control objectives, a switching occurs between these controllers. However, the use of more local controllers not only increases the complexity of the overall control system but also needs to consider the bumpless switching between controllers and windup issues without creating large transient states. In [7], a new method for

ramp rate control of the PV power output oscillations is presented to eliminate the memory effect in the classical averaging techniques. In this paper, power smoothing studies have been carried out over long term intervals, and as a result simplified mathematical models for different parts of the PV-battery system have been used. Furthermore, the ability of the PV system to operate at a point other than the MPP and its coordination with the battery charging/discharging control system has not been discussed. The proposed centralized control strategy in [8] for a PV-battery system is such that the grid-connected inverter always operates at the MPP, and the excess energy produced by the PV is injected into the grid when the battery is fully charged, and therefore, it is not a desirable method from constant power generation point of view. In [9], an intelligent control algorithm for the parallel structure of the battery storage system and wind turbines and PV systems is presented. In this paper, it is assumed that the maximum power point tracking (MPPT) controller for wind turbines and PV arrays always operates at the MPP and lacks any coordination with the battery control system. Moreover, in the proposed algorithm, operational limitations of the batteries such as maximum charge and discharge powers are not considered. In [10]-[11], a control strategy has been proposed for distributed integration of PV and battery energy storage systems (BESSs) in a DC microgrid with variable loads and solar radiation. However, in these works, the coordination between battery and PV converters' controllers has not been discussed during grid-connected condition. Furthermore, the maximum charge/discharge powers of the battery have not been considered in the power management algorithm, and also the system dynamics at the left or right hand sides of the maximum power point of the PV array characteristic have not been studied.

The authors in [12], describe that installing a BESS and curtailing the PV power by operating below the MPP leads to the most economical solution to reduce power fluctuations generated from large grid-connected PV systems. However, the emphasis in the analysis is on investigating the impacts of implementing these methods on the economic benefits that the PV system owner gains, and the authors have provided no dynamical and power electronic based analysis in this study. In [13], a dynamic modeling and control of a grid-connected wind-PV-battery system have been proposed. However, the practical limitations of the battery such as the maximum and minimum of the state of the charge and the maximum charge/discharge power have not been considered. Moreover, the authors do not utilize the power curtailment capability of the PV and wind, MPPT controllers and their coordination with the batteries to achieve further controllability in smoothing of the generated power. An energy management system based on frequency approach is presented in [14], to reduce the variation impacts of the wind/PV energy and the loads via batteries and ultracapacitors. However, in the proposed technique, the limitations of the batteries charge/discharge power, and their state of charge has not been considered. Moreover, it is assumed that the installed PV system operates in its MPP without any power curtailment ability and coordination with the energy storage systems.

In [15], coordinated control strategies have been proposed to provide voltage-frequency (V/f) support in an islanded mode and active-reactive power (P/Q) in grid-connected mode of a microgrid with PV generator and battery storage. However, in this work, the maximum limit of the batteries charge/discharge power has not been considered, and it is also assumed that the PV system always works at its MPP and lacks any coordination with the battery control system. In [16], the challenge of controlling and coordinating of battery energy storage units in a PV storage system has been tackled for smoothing the intermittency of the solar resource and shifting output to more closely match the load profile. In this work, the PV storage system is modeled as a convex optimization problem, and an MPC framework solves the optimization problem using external price signals and predictions of PV output at each time step. The focus of this paper is mainly on system-level studies with simplified models to schedule of power flow of the PV and battery. Therefore, the nonlinear characteristics of the PV array, the MPPT dynamics, and its coordination with the battery control system, have not been discussed in a power electronic-based study. A new energy management method, depending on time and weather conditions, has been proposed for a PV-battery system in [17], by considering of power generations from PV system, residential load variations and electricity price. However, in this work, the power management system is considered only for the battery and the possibility of power curtailment in the PV generator, and its coordination with the battery control system has not been discussed. Moreover, in this paper, the maximum charge and discharge power of the battery are not considered.

In [18], an improved control strategy has been proposed for a grid connected hybrid PV/BESS for mitigating PV farm output power fluctuations. In this work, a feedback controller for BESS state of charge (SOC) is proposed, where the control parameters are optimized using genetic algorithm. However, in this study, the coordination between MPPT and battery control system has not been discussed. Moreover, in this work, long-term studies in the resolution of one sample per minute have been carried out with simplified models in which the fast dynamics of the control system in power electronic converters are not visible. A smoothing control method for reducing wind/PV output power fluctuations and regulating battery state of charge (SOC) has been proposed in [19]. A main feature of this work is to propose the SOC control strategy for large-scale BESS instead of small-scale BESS-based smoothing. However, in this paper, it is assumed that renewable-energy sources operate at their MPPs, and the possibility of their coordination with the battery storage system has not been discussed. In [20], a power management system has been proposed for a smart grid-connected microgrid including diesel, battery storage, and solar plants. However, in this study, the power curtailment ability of PV generators has not been considered, and it is assumed that any mismatch between the smoothing index and BESS power limits would be supplied or absorbed by the grid. Furthermore, only long-term studies with sampling of every 5 minutes have been taken into account and higher precision studies of the level of power electronics circuits' dynamics and transients have not been made.

A rule-based control scheme is proposed in [21] for integrating a BESS with a PV system. Although, in the proposed method, the operating constraints of the BESS, such as the state of charge limits, charge/discharge current limits and lifetime have been considered, however, the coordination between the MPPT and the battery as well as the power curtailment capability of the PV arrays have not been considered. In addition, the studies are of long-term type with large sampling intervals, which have been done via simplified mathematical models that are not capable of representing the dynamic and transient phenomena of power converters. In [22], the problem of power smoothing for a combined wind and PV system has been studied using a battery storage system. In this work, a discrete-time Kalman filter-based method has been used to smooth the battery-generated reference signal and limit the total output power fluctuation. Simplified models are used in this paper, and the coordination between the MPPT and the battery charging/discharging control system has not been discussed. A detailed power electronic based study has been made for a microgrid consisting of PV, hydro generator and battery storage system with the capability of frequency regulation, voltage regulation, power management and load leveling in [23]. However, in this work it is assumed that the PV system always operates at the MPP, and all the power management and regulation tasks are assigned to the battery storage system. In addition, battery system constraints such as minimum and maximum SOC, and maximum charge/discharge power are not considered. In [24], a control strategy for the stable operation of a DC microgrid consisting of PV and a battery storage system has been proposed. In this work, it is assumed that the photovoltaic array

operates constantly at the MPP without any power curtailment ability or coordination with the battery control system. Hence, the critical case in which the battery is fully charged, and the PV generator has the excess power, has not been considered. In [25], [26], a combined energy storage system, including a battery pack and a capacitor bank, has been used to smooth the power fluctuations of a solar power plant. The proposed approach in this work has the ability of power curtailment of the photovoltaic system. However, this paper uses a linear model of the photovoltaic array in its analysis and the nonlinear behavior of the PV array, such as the possibility of operating at the right or left side of the MPP on the PV array nonlinear power-voltage (P-V) curve has not been considered. The proposed power management algorithms in these works are of centralized type by which the reference signals of different units within microgrid are determined by a single algorithm. A combined energy storage system, including battery and diesel generator is used in [27] to smooth the power fluctuations of an islanded PV system. In this work, it is assumed that the PV array operates at the MPP without power curtailment ability and lacks any coordination with the battery and diesel generator control system.

In [28], a Petri net-based power management system for a PV system, including the battery energy storage and super-capacitors has been proposed. The studies are of long-term type, and power electronic details, the design of local controllers and the system dynamics during limiting PV array power for operation on the left or right of the MPP are not studied. A BESS is used to smooth the output power fluctuations of a PV system in [29]. In this paper, to generate the grid reference power signal, a new computational method for the averaging of the power generated from the PV system is used. In this work, no discussion is provided about the critical cases in which the PV system has a shortage or excess in production, and the battery cannot inject or absorb power. The studies are of long-term type, and simplified models have been used for different parts of the PV-battery system. In [30], a centralized energy management system is proposed for a microgrid consisting of PV, supercapacitors, and batteries. In the proposed method, to reduce the PV output power generation, the operating point of PV array is shifted from MPP to the right of this point, by a switching mechanism from MPPT controller to another algorithm called the power limiter. From the drawbacks of using the switching method between different controllers to change the operating point of the PV array on the P-V curve is that, when the PV array operates with one controller, the other controller, based on the received error signal, continues to generate its output signal. This causes that the calculated operating point by the non-active controller to be far away from its desirable value, and when it is again connected to the system, large transient states are created. In [31]-[34], the problem of constant power supplying to the grid has been introduced in the PV generators. These papers do not use any energy storage system such as batteries, and the constant power generation is attempted using only by changing the operating point of MPPT to the left or right of the maximum power point. However, according to the analysis made in [12], the combination of the PV generators with power curtailment ability and energy storage systems such as batteries is the most economical and efficient solution to reduce output power fluctuations of a PV system. A PV system consisting of the battery and supercapacitor storage systems with a centralized and coordinated control system between solar arrays and storage systems has been studied in [35]. In this paper, the case in which the solar arrays generate excess power, and the battery and supercapacitor are fully charged, is handled by changing the operating point of solar array to a point other than the MPP on the P-V curve. However, the mechanism of this operating point shifting on the P-V curve of the solar arrays has not been given with an in-depth analysis. In [36], a multifunctional control of a grid-connected PV/battery inverter is proposed with both power quality compensation and power management system. In this work, the battery is connected directly to the DC bus without any bidirectional converter to control the battery power flow. The proposed power management system is of centralized type lacking any power curtailment capability in the PV generator MPPT. Furthermore, the maximum limit of the battery charge/discharge power has not been considered in the proposed power management system. A fuzzy-logic based control strategy for the battery of the plug-in hybrid electric vehicles has been proposed in [37] to mitigate the voltage fluctuation of a distribution system fed by the PV power generators. Furthermore, the PV interface inverter is equipped with the reactive power compensation capability which enhances the feeder voltage profile during cloud transients. However, in this work, the batteries' operational limits such as maximum charge/discharge power and SOC have not been considered. Furthermore, there is no coordination between battery and PV control systems and it is assumed that the PV generators operate in the MPP point without any power curtailment capability. In [38], a centralized and hysteresis-based energy management system has been proposed to control the DC bus voltage of a grid-connected PV/battery system to reduce the negative influences of the power fluctuations of a PV generation system. In this work, it is assumed that the PV generator always works in MPP without power curtailment capability. Furthermore, the battery limitations such as the maximum/minimum SOC and maximum charge/discharge powers have not been considered.

Motivated to the abovementioned shortcomings and literature review, this paper proposes a cooperative control strategy in a distributed structure between battery charge/discharge control system and PV MPPT controller. Most of the past works described in the literature have a battery energy storage system connected to the PV or wind systems, without any coordination with the MPPT controller of the PV or wind turbines. Furthermore, in some cases the batteries' operational limitations have not been handled during control systems design. While a successful closed-loop design needs to consider major control limitations. In most cases, the proposed power management systems are developed in a centralized manner with some shortcomings such as higher complexity, less reliability, no plug-and-play feature, and switching requirement among various local controllers leading to consider bumpless switching scheme design. Finally, in most cases, long-term studies of an order of minutes and hours based on simplified models have been proposed, which are unsuitable to investigate short-term dynamical behaviors of the overall power electronic based control system. To address all these issues, this paper proposes the use of a cooperative and distributed control strategy between PV array and BESS controllers in a grid-tied PV-battery system. The use of such a cooperative control provides extra functionality, flexibility and controllability of the overall system to achieve better integration of the PV-battery systems for the distribution and transmission systems. The current work fulfills the proposed gaps by presenting an in depth power-electronic based analysis of such a coordination. In addition, this paper aims to emphasize the concept of conversion of nondispatchable renewable-energy sources such as PV units, which are typically operated to extract the maximum possible power, to dispatchable units (e.g. diesel generators) that can be fully controlled. The main contributions of this work are summarized as follows:

- Detailed and step-by-step design, modeling and local controller synthesis of all PV/battery subsystems at the device-level studies of power electronic circuits are presented.
- A new power management control strategy with a distributed structure is proposed which is able to regulate PV/battery output power in a constant setpoint.
- The proposed control strategy considers all the batteries' operational limitations such as maximum/minimum SOC and maximum charge/discharge power, and power curtailment capability

of the PV arrays with the ability of shifting the operating point to the left or right hand side of the MPP.

The remainder of the paper is organized as follows: In Section 2, the overall structure of the PV-battery system under study is described as well as, modeling, design and local controllers' synthesis for its subsystems. Section 3 deals with the proposed distributed power management controller. In Section 4, the simulation results of the system under study are presented in various scenarios and over a wide range of operating points. Finally, concluding remarks are made in Section 5.

2. Modeling, design and local controllers' synthesis of the PV-battery system

Figure 1 illustrates the general schematic diagram of the studied system in this paper, which includes: a PV array, a PV bus capacitor, C_{PV}, to hold a constant voltage on the PV array side, a DC/DC boost converter to increase the DC bus voltage, a DC bus capacitor, C_{DC}, to keep the voltage constant at the output side of the boost converter and the inverter DC bus, a three-phase voltage source inverter for converting DC power to AC power, a three-phase RL filter to remove harmonics on the network side, a bi-directional DC-DC converter between the inverter DC link and the battery power storage system.

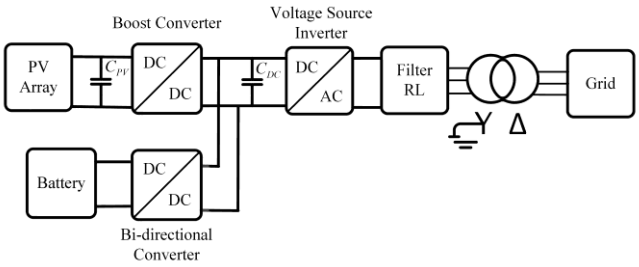

Fig. 1. The schematic diagram of a grid-connected three-phase double-stage PV-battery system

2.1. Modeling, design and local controller synthesis for PV generater

Figure 2 shows the equivalent circuit of the PV array used in Figure 1 consisting of N_p parallel PV strings each of which contains N_s series connected PV modules [39].

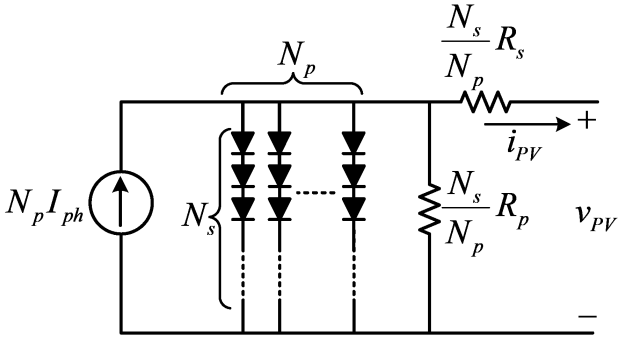

Fig. 2. The equivalent circuit of a PV array

According to Figure 2, the relationship between the output voltage v_{PV} and current i_{PV} of the PV array can be expressed by (1)-(4).

$$i_{PV} = N_p I_{ph} - N_p I_o \left[\exp\left(\frac{v_{PV} + \frac{N_s}{N_p} R_s i_{PV}}{a N_s N_{se} \frac{kT}{q}} \right) - 1 \right] - \frac{v_{PV} + \frac{N_s}{N_p} R_s i_{PV}}{\frac{N_s}{N_p} R_p} \quad (1)$$

$$I_o(T) = \frac{I_{sc} + K_I (T - T_{STC})}{\exp\left(\frac{V_{oc} + K_V (T - T_{STC})}{a N_{se} \frac{kT}{q}} \right) - 1} \quad (2)$$

$$I_{ph} = \frac{G}{G_{STC}} \left(I_{ph,STC} + K_I (T - T_{STC}) \right) \quad (3)$$

$$T = T_a + (NOCT - 20) \frac{G}{800} \quad (4)$$

where $T_{STC} = 25 + 273.15\ ^\circ\text{K}$ and $G_{STC} = 1000\,\text{W}/\text{m}^2$ are the PV module temperature and irradiation levels at the standard test conditions (STC), respectively. The T_a is the ambient temperature considered as $25\ ^\circ\text{C}$ in this study. The other parameters used in (1)-(4) with their descriptions and values for the KC200GT PV module are given in Table 1 [39].

Table 1. The PV module KC200GT parameters

Symbol	Quantity	Value
P_{mpp}	Maximum power	$200\,\text{W}(+10\%-5\%)$
V_{mpp}	Maximum power voltage	$26.3\,\text{V}$
I_{mpp}	Maximum power current	$7.61\,\text{V}$
V_{oc}	Open circuit voltage	$32.9\,\text{V}$
I_{sc}	Short circuit current	$8.21\,\text{A}$
K_V	Temperature coefficient of V_{oc}	$-0.123\,\text{V}/^\circ\text{C}$
K_I	Temperature coefficient of I_{sc}	$0.00318\,\text{A}/^\circ\text{C}$
$NOCT$	Nominal operating cell temperature	$47\ ^\circ\text{C}$
N_{se}	Number of series cells	10
I_o	saturation current at STC	$9.825\times10^{-8}\,\text{A}$
I_{ph}	Photo current at STC	$8.214\,\text{A}$
a	Diode ideality factor	1.3
R_s	PV module series resistance	$0.221\,\Omega$
R_m	PV module parallel resistance	$415.405\,\Omega$
q	Elementary charge	$1.6\times10^{-19}\,\text{C}$
k	Boltzmann's constant	$1.38\times10^{-23}\,\text{J}/^\circ\text{K}$

Since the PV-battery system under study is considered for the

nominal power $P_{array}=100\text{kW}$, the array voltage $V_{array}=280\text{V}$, the ambient temperature $T_a=25+273.15\ ^\circ\text{K}$ and the radiation level of $G=G_{STC}=1000\text{W}/\text{m}^2$, and on the other hand, the specifications of the PV module KC200GT in Table 1 are provided at STC, we initially obtain an estimation of the module parameters V_{mpp} and P_{mpp} at the ambient temperature of $T_a=25+273.15\ ^\circ\text{K}$ using translational formulas in (5)-(8) [39]-[40].

$$T=T_a+(NOCT-20)\frac{G}{800}= 25+273.15+(47-20)\frac{1000}{800}=58.8+273.15\ ^\circ\text{K} \quad (5)$$

$$V_{mpp}(T)=V_{mpp}+K_V(T-T_{STC})= 26.3-0.123(58.8-25)=22.14\text{V} \quad (6)$$

$$I_{mpp}(T)=I_{mpp}+K_I(T-T_{STC})= 7.61+0.00318(58.8-25)=7.72\text{A} \quad (7)$$

$$P_{mpp}(T)=V_{mpp}(T)I_{mpp}(T)= 22.14\times 7.72=170.94\text{W} \quad (8)$$

where $V_{mpp}(T)$, $I_{mpp}(T)$ and $P_{mpp}(T)$ are the MPP voltage, current and power of the PV module at the module temperature T calculated by (4). Now, an estimation of the PV array parameters N_p and N_s can be obtained by (9)-(10).

$$N_s=\frac{V_{array}}{V_{mpp}(T)} \quad (9)$$

$$N_p=\frac{P_{array}}{N_s P_{mpp}(T)} \quad (10)$$

Using (9)-(10) and simulating the P-V curve of the PV array via (1)-(4), the dimensions of the PV array are selected as $N_s=12$ and $N_p=44$.

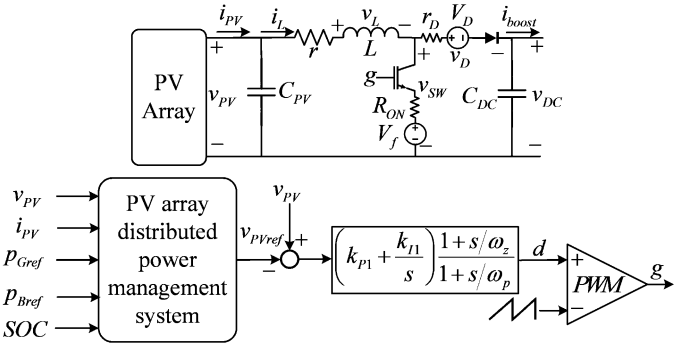

Fig. 3. The boost converter topology and its control system

To control the PV array output power, a dc-dc boost converter is used that the distributed energy management controller of the PV generator determines its input voltage reference value v_{PVref}. Next, the converter local controller determines the proper switching duty cycle d. Details of the distributed controller of the external control layer are given in Section 4. Figure 3 shows the PV array boost converter topology and the corresponding control system. Hereafter, in all power electronic converters, diodes and transistors are modeled by a voltage source and a series resistance during their turn on. In Figure 3, $r=1\text{m}\Omega$ is the internal resistance of the inductor, $R_{ON}=1\text{m}\Omega$ and $V_f=1\text{V}$ are the IGBT turn-on resistance and forward voltage, respectively, $r_D=1\text{m}\Omega$ and $V_D=0.8\text{V}$ are the diode turn-on resistance and forward voltage drop, respectively, v_L and i_L are the inductor voltage and current, respectively, d is the converter duty cycle, v_{PV} and i_{PV} are the PV array voltage and current, respectively. According to Figure 3, and using the averaging and linearization techniques [39], the transfer function of $\Delta v_{PV}(s)/\Delta d(s)$ is obtained as (11):

$$\frac{\Delta v_{PV}(s)}{\Delta d(s)}=\frac{-k_2}{LC_{PV}s^2+k_1C_{PV}s+1} \quad (11)$$

where $k_1=DR_{ON}+r+(1-D)r_D$ and $k_2=V_D+V_{dc}-V_f+(r_D-R_{ON})I_L$. $V_{dc}=700\text{V}$ is the DC link nominal voltage and $I_L=100kW/280V=357.14\text{A}$ is the boost converter inductor nominal current. The switching frequency of the converter is set to $f_s=5\text{kHz}$. Using the steady-state analysis of the converter at the nominal operating point [42], the values of the capacitor C_{PV} and the inductor L are calculated by (12)-(14):

$$D=\frac{V_{PV}-(r+r_D)I_L-V_D-V_{dc}}{(R_{ON}-r_D)I_L+V_f-V_D-V_{dc}}= \frac{280-(0.001+0.001)357.14-0.8-700}{(0.001-0.001)357.14+1-0.8-700}=0.6 \quad (12)$$

$$C_{PV}=\frac{\Delta i_{L,p-p}}{8f_s\Delta v_{PV,p-p}}=\frac{0.1\times 357.14}{8\times 5000\times 0.01\times 280} =318.87\,\mu F\cong 400\,\mu\text{F} \quad (13)$$

$$L=\frac{V_{PV}DT_s}{\Delta i_{L,p-p}}=\frac{280\times 0.6\times 1/5000}{0.1\times 357.14}= 944.47\,\mu H\cong 1\text{mH} \quad (14)$$

In (13)-(14), the maximum percentages for the current and voltage ripples are considered as 10% and 1%, respectively. Using (11) and controller design method in the frequency-domain [39], and assuming the cut-off frequency of 0.1 switching frequency and the phase margin of 52 degrees, the coefficients of the local controller in Figure 3 are calculated as $k_{P1}=0.0015$, $k_{I1}=0.4712$, $\omega_z=1081.7$ and $\omega_p=9123.8$.

2.2. Modeling, design and controller synthesis of grid-connected inverter

Figure 4 illustrates the control system block diagram of the grid-tied inverter used in Figure 1 [39]. In this figure, $r_{on}+R_f=0.011\Omega$ is the effective resistance of the inverter consisting of the output filter resistance $R_f=0.01\Omega$ and the equivalent turn-on resistance of the inverter transistors $r_{on}=0.001\Omega$, L_f indicates the inductance of the output filter inductor, v_{sq} and i_q are the q-axis components of the voltage and currents of the inverter AC side in the dq frame and v_{sd} and i_d are the d-axis components. m_d and m_q are the d and q components of the sinusoidal pulse width modulation indices m_a, m_b

and m_c in the dq frame. C_{DC} is the capacitance of the DC link capacitor. The switching frequency of the inverter is $f_s = 5\text{kHz}$ and its line-to-line output voltage and rated power are 400 volts and 100 kilowatts, respectively. The grid fundamental frequency is 50 Hz. The values of L_f and C_{DC} are calculated by (15)-(16):

$$L_f = \frac{2V_{dc}T_s}{\Delta i_{p-p}} = \frac{2\times 700\times 1/5000}{0.1\times\left(\frac{100kW}{400\sqrt{3}}\times\sqrt{2}\right)} = 1.5\,\text{mH} \quad \textbf{(15)}$$

$$C_{DC} = \frac{P_n T_s}{V_{dc}\Delta v_{dc,p-p}} = \frac{100kW\times 1/5000}{700\times(0.01\times 700)} = 4.1mF \cong 5\,\text{mF} \quad \textbf{(16)}$$

In (15)-(16), the maximum current and voltage ripple percentage is considered to be 10% and 1%, respectively. According to Figure 4, the currents' dynamics of the AC side inverter in the dq frame are described by (17)-(18) [39].

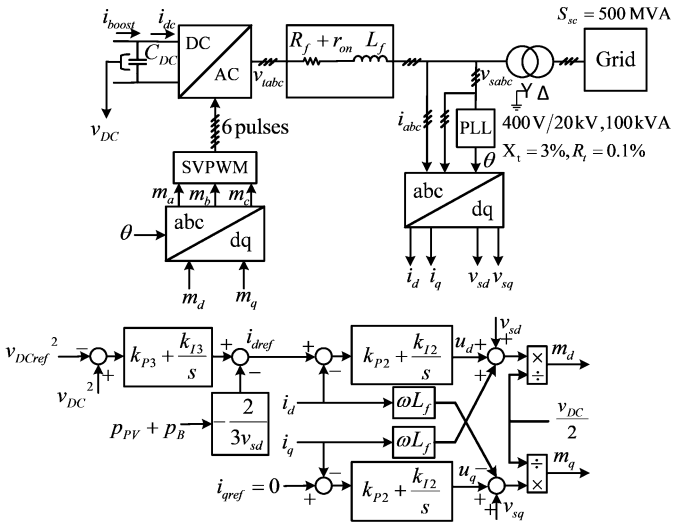

Fig. 4. The overall control block-diagram of the grid-tied inverter

$$L_f\frac{di_d}{dt} = v_{td} - v_{sd} - (R_f + r_{on})i_d + L_f\omega i_q \quad \textbf{(17)}$$

$$L_f\frac{di_q}{dt} = v_{tq} - v_{sq} - (R_f + r_{on})i_q - L_f\omega i_d \quad \textbf{(18)}$$

where ω is the grid angular frequency and v_{td} and v_{tq} are calculated via (19)-(20).

$$v_{td} = m_d\frac{v_{DC}}{2} \quad \textbf{(19)}$$

$$v_{tq} = m_q\frac{v_{DC}}{2} \quad \textbf{(20)}$$

Due to the existence of the terms $L_f\omega i_d$ and $L_f\omega i_q$ in (17)-(18), the dynamics of i_d and i_q are coupled to each other. To decouple these dynamics, the control inputs m_d and m_q are defined as (21)-(22).

$$m_d = \frac{2}{v_{dc}}(u_d - L_f\omega i_q + v_{sq}) \quad \textbf{(21)}$$

$$m_q = \frac{2}{v_{dc}}(u_q + L\omega i_d + v_{sq}) \quad \textbf{(22)}$$

where u_d and u_q are the new control inputs. By substituting (21)-(22) in (19)-(20) and then replacing v_{td} and v_{tq} from (19)-(20) in (17)-(18) one can obtain:

$$L_f\frac{di_d}{dt} = -(R_f + r_{on})i_d + u_d \quad \textbf{(23)}$$

$$L_f\frac{di_q}{dt} = -(R_f + r_{on})i_q + u_q \quad \textbf{(24)}$$

The equations in (23)-(24) are two first-order decoupled linear systems in which i_d and i_q can be controlled by u_d and u_q. Accordingly, in Figure 4, the coefficients of the current-loop controllers $k_{P2} = 3.7235$ and $k_{I2} = 9138.8$ are calculated using the frequency-domain design method with the assumption of the cut-off frequency of 0.1 switching frequency and a phase-margin of 52 degrees. According to Figure 4, by neglecting of the power losses in the inverter and its output series reactor, the dynamic of the DC link voltage can be described as (25).

$$C_{DC}\frac{dv_{DC}}{dt} = i_{boost} + i_B - \frac{3v_{sd}i_d}{2v_{DC}} \quad \textbf{(25)}$$

By multiplying both sides of (25) to v_{DC}, one can obtain:

$$C_{DC}v_{DC}\frac{dv_{DC}}{dt} = v_{DC}i_{boost} + v_{DC}i_B - \frac{3v_{sd}i_d}{2} \quad \textbf{(26)}$$

By neglecting of the losses of the boost converter between the PV array and the voltage source inverter, as well as the losses of the bidirectional converter between the battery and the DC link of the inverter, one can write $v_{DC}i_{boost} + v_{DC}i_B = p_{PV} + p_B$ in which p_B and p_{PV} are the generated powers by the battery and PV array, respectively. Now (26) can be rewritten as (27):

$$\frac{1}{2}C_{DC}\frac{dv_{DC}^2}{dt} = p_{PV} + p_B - \frac{3v_{sd}i_d}{2} \quad \textbf{(27)}$$

In (27), v_{dc}^2 is the output variable that can be controlled by the variable i_d. By taking a Laplace transform from (27) and considering $p_{PV} + p_B$ as the disturbance term, we have:

$$\frac{v_{DC}^2(s)}{i_d(s)} = -\frac{3v_{sd}}{C_{DC}s} \quad \textbf{(28)}$$

Using (28), and considering a feedforward path to reduce the disturbance effect of $p_{PV} + p_B$, the block diagram of the outer DC link voltage loop control of the inverter can be represented as Figure 5.

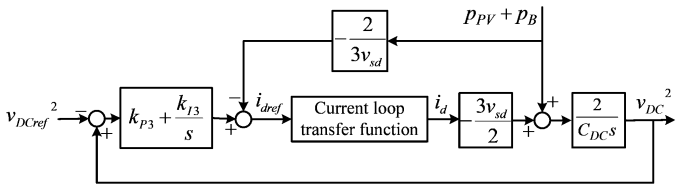

Fig. 5. The block diagram of the inverter DC link voltage loop control

Since in the multi-loop control systems, the bandwidth of the inner loop is considerably smaller than the outer loop (with a ratio of 0.1), the internal transfer function can be set to one, from the external control loop viewpoint. With this assumption, the uncompensated open-loop transfer function is expressed as (28). The voltage controller coefficients $k_{P3}=0.0013$ and $k_{I3}=0.311$ are obtained by the frequency domain controller synthesis with a cutoff frequency of 0.01 converter switching frequency (0.1 frequency of the current-loop bandwidth) and the phase margin of 52 degrees.

2.3. Modeling, design and local controller synthesis for the battery pack

In this paper, the Litium-ion battery cell 850-mAh TCL PL-383562 is used for modeling. Figure 6, shows the electrical equivalent circuit of the battery array using the circuit model given in [43] for a battery cell. In this figure, the battery array is consisting of N_{PB} parallel rows each of which consisting of N_{SB} series connected battery cells. Assuming that V_{BATT}, I_{BATT} and P_{BATT} are the nominal values of the battery cell voltage, current and power, respectively, if the required nominal battery array power and voltage are considered as P_B and V_B, then the values of N_{PB} and N_{SB} can be calculated by (29)-(30).

$$N_{SB}=\frac{V_B}{V_{BATT}} \quad \textbf{(29)}$$

$$N_{PB}=\frac{P_B}{N_{SB}P_{BATT}} \quad \textbf{(30)}$$

In Figure 6, v_{OC} is the open-circuit voltage, $C_{Capacity}=3060\,\mathrm{F}$ is the usable capacity of the battery, $R_{self-discharge}=10^6\,\Omega$ is the battery self-discharge resistance used to indicate the energy losses of the batteries when they are kept in the fully-charged state for a long time. SOC Indicates the battery state of charge or in other words, the percentage of the existing battery charge with respect to its maximum capacity. The series resistance $R_s(SOC)$ represents the momentary voltage drop of the step response. The model is composed of two parallel RC networks, in which $R_{TS}(SOC)$ and $C_{TS}(SOC)$ model a part of the battery step response with small time constant, and $R_{TL}(SOC)$ and $C_{TL}(SOC)$ indicate the battery step response dynamic with a large time constant.

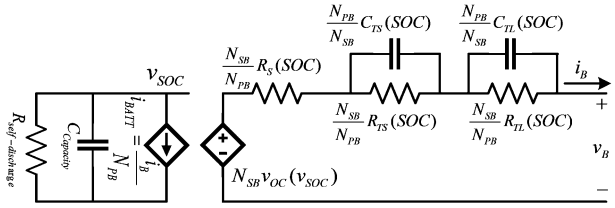

Fig. 6. The equivalent circuit of the battery pack used in Fig. 1

The values of the battery cell parameters are given in (31)-(36), [43].

$$v_{oc}(SOC)=-1.031e^{-35SOC}+3.685+0.2156SOC-0.1178SOC^2+0.3201SOC^3 \quad \textbf{(31)}$$

$$R_s(SOC)=0.1562e^{-24.37SOC}+0.07446 \quad \textbf{(32)}$$

$$R_{TS}(SOC)=0.3208e^{-29.14SOC}+0.04669 \quad \textbf{(33)}$$

$$C_{TS}(SOC)=-752.9e^{-13.51SOC}+703.6 \quad \textbf{(34)}$$

$$R_{TL}(SOC)=6.603e^{-155.2SOC}+0.04984 \quad \textbf{(35)}$$

$$C_{TL}(SOC)=-6056e^{-27.12SOC}+4475 \quad \textbf{(36)}$$

Based on the information in the battery cell catalog, the nominal values of the battery cell voltage and current are considered as $V_{BATT}=3.7\,\mathrm{V}$ and $I_{BATT}=850\,\mathrm{mA}$ [44]. Since the rated power of the PV system is 100 kW, the capacity of the storage system is considered to be about 30% of the output power of the PV system, i.e., $P_B=30\,\mathrm{kW}$ [27]. As a result, by assuming a nominal voltage of $V_B=280\,\mathrm{V}$ for the battery array, the number of parallel rows and the number of battery cells in each row, are obtained by (29)-(30) as $N_{PB}=126$ and $N_{SB}=76$.

When needed, the BESS injects or absorbs the required power to the DC link to cause the PV system to provide a constant and stable power to the grid. In order the BESS to be able to do this, it needs a bi-directional converter. The bi-directional converter topology for the battery used in this paper is shown in Figure 7.

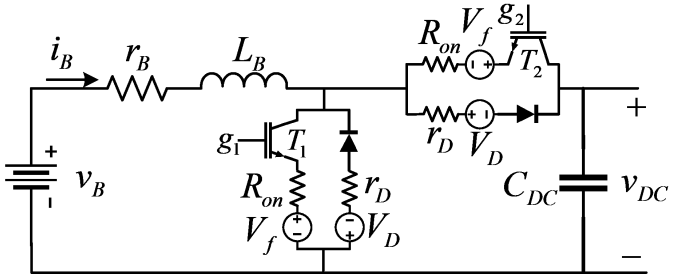

Fig. 7. The bidirectional converter topology used in Fig. 1

According to Figure 7, if the switch T_2 is turned off permanently, and the switch T_1 is switched on and off with high frequency, the current flows from the battery to the DC link and the battery is discharged. If the switch T_2 is turned on and off and the switch T_1 is turned off permanently, the current flows from the DC link to the battery and in this case, the battery is charging. The bi-directional converter control system is shown in Figure 8. According to this figure, at first, the grid reference power p_{Gref}, the battery SOC, and the PV output power are fed to the battery distributed power management controller as input signals. Next, the distributed controller generates the battery reference power p_{Bref}. Using p_{Bref} and the battery voltage v_B, the battery reference current is calculated as $i_{Bref}=p_{Bref}/v_B$.

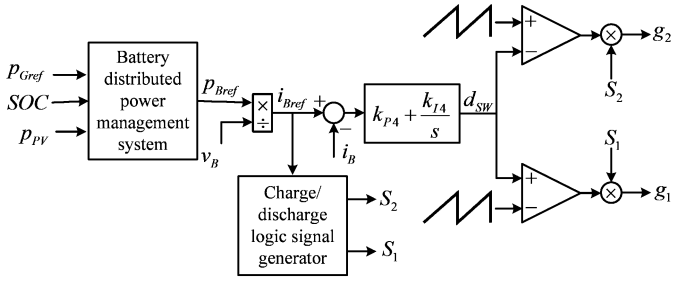

Fig. 8. The bidirectional converter control system

By passing the error signal from a PI controller, the switch duty cycle d_{SW} is calculated. d_{SW} is the required duty cycle to generate the gate pulses of the switch T_1 to discharge the battery. On the other hand, the duty cycle of the switch T_2 to charge the battery is equal to $1-d_{SW}$. Therefore, to produce the required gate pulses for the switches T_1 and T_2 a complementary comparative drive system with the same sawtooth carrier wave is used. Since we want to ensure that only one of the switches T_2 or T_1 is switched on during the battery charging or discharging states, a logical hysteresis-like controller is used to generate suitable activating signals S_1 and S_2 as shown in Figure 9.

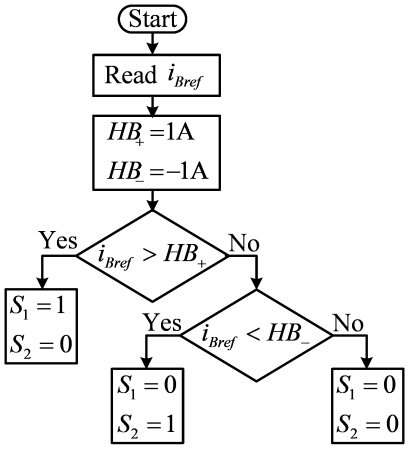

Fig. 9. The hysteresis-like logical controller for the battery bidirectional converter

In Figure 9, a hysteresis band is defined for the battery reference current signal i_{Bref} with the upper and lower limits of HB_+ and HB_-, respectively. If i_{Bref} is within this band, it means that the power generated by the PV array is equal to the power required to be delivered to the grid. If i_{Bref} is greater than the upper limit HB_+, then the power generated by the PV array is less than that of the power required to be delivered to the grid and the battery is discharging. Finally, if i_{Bref} is less than the lower bound HB_-, then the power generated by the PV array is greater than the power required to be delivered to the grid, and the battery is being charged.

To design the current controller in Figure 8, we need to obtain the bidirectional converter transfer function from switch duty cycle to the inductor current. According to Figure 7, and considering that the output voltage of the bidirectional converter v_{DC}, which is the DC bus voltage of the inverter as well, is kept constant by the inverter controllers at the reference value of v_{DCref}, thus the output of the bidirectional converter in Figure 7 can be considered as a voltage source similar to converter's input. In this case, when switch T_1 is closed and the switch T_2 is open, the state equation for the inductor current dynamic is described as (37):

$$v_B = r_B i_B + L_B \frac{di_B}{dt} + R_{ON} i_B + V_f \tag{37}$$

On the other hand, when the switch T_1 is open and the switch T_2 is closed, the state equation of the converter is described as (38)

$$v_B = r_B i_B + L_B \frac{di_B}{dt} + r_D i_B + v_B + v_{dc} \tag{38}$$

Now, by combining the dynamics (37) and (38), and using averaging and linearization techniques, the transfer function from $\Delta d_{sw}(s)$ to $\Delta i_B(s)$ is obtained as (39).

$$\frac{\Delta i_B(s)}{\Delta d_{sw}(s)} = \frac{(r_D - R_{ON})I_B + V_D + V_{dc} - V_f}{L_B s + r_B + D_{sw} R_{ON} + (1 - D_{sw}) r_D} \tag{39}$$

where $I_B = 30\text{kW}/280\text{V} = 107.14\text{A}$ is the battery current in the rated operational conditions. The value of the converter's duty cycle and the size of the inductor L_B can be obtained using the converter analysis in the steady-state conditions [39] via (40)-(41).

$$D_{sw} = \frac{V_B - (r_D + r_B)I_B - V_{dc} - V_D}{V_f - V_D - V_{dc} + (R_{ON} - r_D)I_B} = \frac{280 - (0.001 + 0.001)107.14 - 700 - 0.8}{1 - 0.8 - 700 + (0.001 - 0.001)107.14} = 0.6 \tag{40}$$

$$L_B = \frac{(V_{dc} - V_B) D_{sw} T_s}{\Delta i_{B,\,p-p}} = \frac{(700 - 280) \times 0.6 \times 1/5000}{0.1 \times 107.14} = 3.1\text{mH} \tag{41}$$

where $f_s = 1/T_s = 5\text{kHz}$ is the converter switching frequency. Equation (39) represents a first-order linear system for which the current controller parameters of Figure 8, $k_{P4} = 0.0111$ and $k_{I4} = 27.3016$ are designed by assuming a cutoff frequency of 0.1 of the converter switching frequency and the phase margin of 52 degrees.

3. The proposed distributed power management control system

Power management systems in microgrids can be divided into three large categories of centralized control, decentralized control and distributed control [11], [45]. Centralized control system based on a communication platform receives and analyzes information from all units in the microgrid and sends appropriate power reference signals, based on the control objectives defined for the microgrid, to the local controllers of each of microgrid units. One of the advantages of this approach is the possibility of using optimization algorithms to obtain the best control decisions in terms of defined control objectives and available operational constraints. One of the drawbacks of this control scheme is that with the increase of the number of resources in the PV systems, the complexity of the power management algorithm increases

as well. Moreover, with the addition of new units to the system, to have a correct function, it is necessary that the power management algorithm and its settings are changed. Figure 10(a) illustrates the structure of a centralized control in a PV-Battery system in which the control objective is to supply the active power p_{Gref} demanded by the grid. As it can be seen from this figure, the central controller receives the information from PV and battery sources, and according to the amount of requested power p_{Gref}, determine suitable power reference signals to each of these sources.

In a decentralized control structure, each unit is controlled only by the local controllers and based on the local information, without any need for awareness of the operation of other units. One of the advantages of such a control structure is its no requirement for any communication platform. Furthermore, in such a control structure, it is easy to integrate new units without making any major changes to the control system settings. Unfortunately, due to the strong couplings among various units in the grid, this type of control architecture is not feasible in practice, and for an accurate operation of the entire system, a minimum level of coordination between local controllers is always required. As a result, a compromise between the centralized and decentralized control systems is distributed control systems. This type of control structure reduces the complexity of the centralized control structure and, like decentralized control systems, creates a degree of autonomy and independence between different units and increases the reliability of the system against the outgoing of one of the units or the addition of a new unit. However, it still needs a communication platform to exchange information between different controllers. In this paper, a distributed control structure, as shown in Figure 10(b), is used for a PV-battery system for generating requested power p_{Gref} by the remote control and dispatching center.

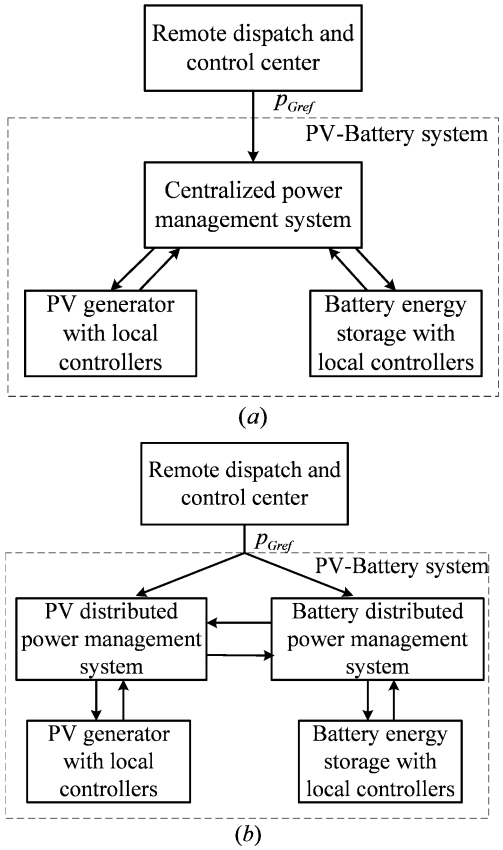

Fig. 10. Various supervisory control schemes, (a) centralized control, (b) distributed control

Figures 11 and 13 show the details of the distributed control algorithms for the battery storage system and PV generator. Figure 11 illustrates how the battery's reference power signal p_{Gref} is generated.

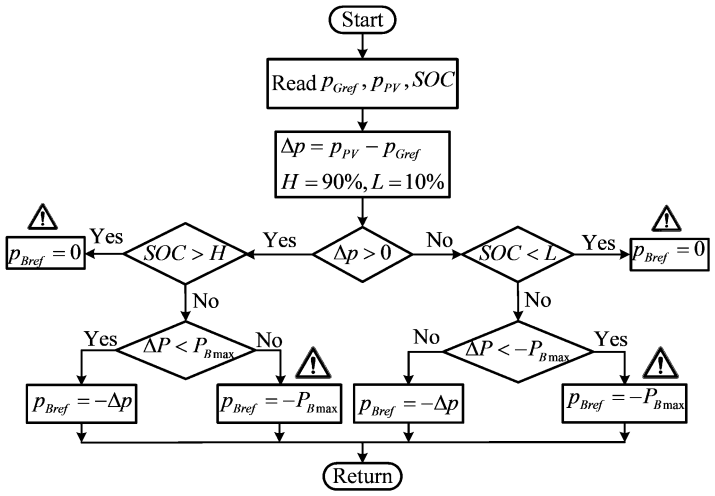

Fig. 11. The battery distributed control flowchart

In Figure 11, the PV array instantaneous power p_{PV} is compared with the grid reference power p_{Gref} and the error signal is calculated as $\Delta p = p_{PV} - p_{Gref}$. Furthermore, to increase battery life and prevent its overcharging or over discharging, the higher and lower bonds of H and L are considered for the battery charge level SOC. The parameter $P_{B\max} = 30\,\text{kW}$ in the flowchart indicates the battery nominal power.

If Δp is positive, it means that the power generated by the PV array is greater than the power required to be delivered to the grid, and it is necessary the excess power to be directed toward the battery. Now, if $SOC > H$, the battery is fully charged and cannot absorb the excess power, and as a result, the battery reference power is set to zero, i.e., $p_{Bref} = 0$. Otherwise, if $\Delta p < P_{B\max}$, it means that the battery can absorb all of the extra power, and $p_{Bref} = -\Delta p$. If $\Delta p > P_{B\max}$ it means the battery can only absorb $P_{B\max} = 30kW$ and as a result $p_{Bref} = -P_{B\max}$.

If Δp is negative, it means that the power generated by the PV array is less than the power needed to be delivered to the grid, and the power shortage should be supplied by the battery. Now, if $SOC < L$, then the battery cannot be discharged, and its reference power signal is set to zero, i.e., $p_{Bref} = 0$. Otherwise, if $\Delta p < -P_{B\max}$, it means that the amount of power shortage is greater than the battery rated power, and the battery can only compensate it up to its rated power 30 kilowatts, and therefore, $p_{Bref} = P_{B\max}$. On the other hand, if $\Delta p > -P_{B\max}$, it means that the amount of power shortage needed to be delivered to the grid is less than the battery rated power, and the battery can compensate all the power shortage. Thus, p_{Bref} is set as $p_{Bref} = -\Delta p$. After determination of p_{Bref}, the amount of power absorption or generation by the battery is adjusted by the local current controller shown in Figure 8.

In Figure 11, there are some critical nodes marked by a danger sign. In these nodes, the situation is such that either excess power generated by the PV array cannot be absorbed by the battery due to its fullness, or only a part of the excess power can be absorbed by the battery because its amount is greater than the battery rated power. In

the case of power shortage, either due to the battery emptiness, it cannot inject any power to the PV system, or only a part of the power shortage can be compensated by the battery because the amount of power shortage is greater than the battery rated power. One of the goals of this paper is to overcome the problem of PV array over-production by coordinating the battery's and PV array's energy management systems in such a way that, if the battery cannot absorb the power, the PV array operating point can be shifted below its maximum power point, to be able to work at lower power levels.

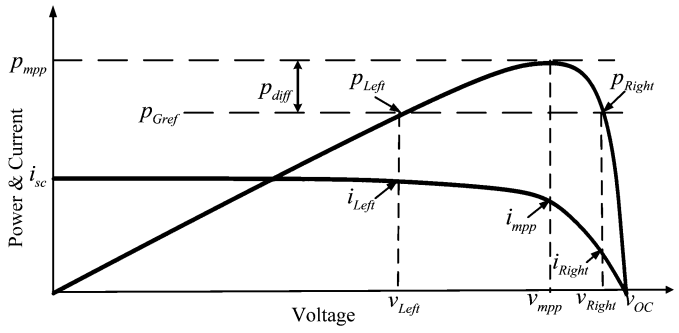

Fig. 12. Power curtailement procedure on the PV array P-V and I-V characteristics

Figure 12 shows that if we reduce the PV array maximum power by an amount of p_{diff}, the problem of overproduction is solved. The value of p_{diff} is a function of the battery charge level. If the battery is full, then $p_{diff} = p_{mpp} - p_{Gref}$ in which p_{mpp} is the maximum power that can be generated by the PV array and p_{Gref} is the grid reference power, i.e., the power should be delivered to the grid. Furthermore, if the battery cab be charged, and the generated excess power is greater than the battery rated power, then p_{diff} is set to be $p_{diff} = p_{mpp} - (p_{Gref} + P_{B\max})$. In Figure 12 it can be seen that if we reduce the maximum power generation of the PV array by an amount of p_{diff}, then two operating points on the left and right sides of the MPP are possible.

These operating points can be obtained by regulating the PV array voltage at a lower value v_{Left} or higher level of v_{Right} with respect to the MPP voltage v_{mpp}. This can be done by the control system of the PV array boost converter shown in Figure 3. Here, we describe the function of the distributed power management system of the PV generator shown in Figure 3, which can solve the problem of PV over-power generation by power curtailment procedure shown in Figure 12. The detail of the proposed distributed control algorithm for PV array is shown in Figure 13. According to the proposed algorithm in this figure, after reading the inputs, the PV array current and voltage increments, i.e., Δi_{PV} and Δv_{PV}, are calculated. Next, the PV array output power is compared with the grid reference power p_{Gref}. If $p_{PV} \le p_{Gref}$, it means that there is no extra production, and therefore, the classic MPPT controller based on the incremental conductance (IC) algorithm is run. However, if $p_{PV} > p_{Gref}$ it means that the PV arrays generate extra power. Now if the battery charge level is more than 90%, i.e., $SOC > 90\%$, then the battery is fully charged and cannot absorb extra power. In this case, we need to curtail PV power generation.

To do this, if our goal is to reach to the operating point on the right side of the MPP, then until $p_{PV} > p_{Gref}$, the reference voltage generated by MPPT, i.e., v_{PVref} is increased with constant step ΔV, and if our goal is to reach the left operating point, it is decreased with constant step ΔV. Now, if the battery charge level is less than 90%, i.e., $SOC < 90\%$, it means that the battery can absorb extra power, but the question arises how much of this excess power can be absorbed by the battery. To answer this question, the produced power by the PV array p_{PV} is compared with the sum of the battery rated power and grid reference power, $P_{B\max} + p_{Gref}$. If $p_{PV} \le p_{Gref} + P_{B\max}$, then the classic MPPT based on IC algorithm is implemented, otherwise if $p_{PV} > p_{Gref} + P_{B\max}$, it means that the battery can absorb only a part of the extra power generation. Now, if the goal is to reach the operating point on the right of MPP, the PV reference voltage v_{PVref} is increased with constant steps of ΔV, and if our goal is to operate on the left of MPP, the reference voltage is decreased.

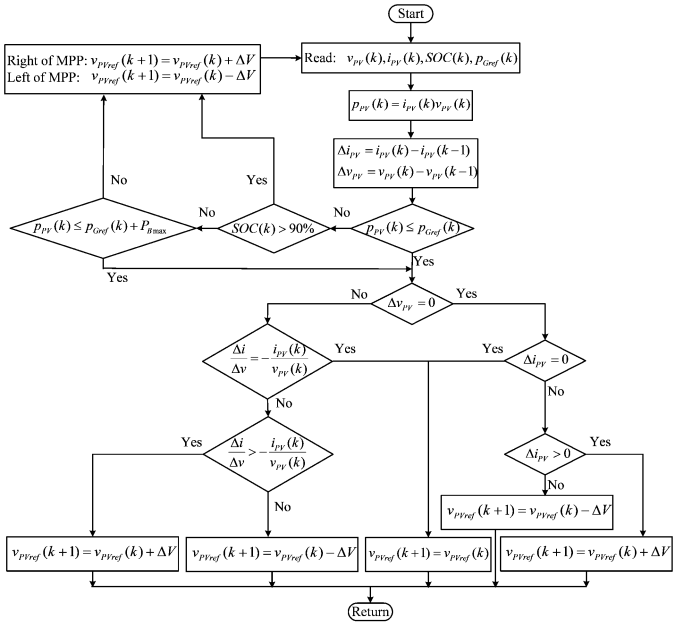

Fig. 13. The distributed control algorithm for PV array

4. Results and discussion

Since the solar radiation can vary for different reasons such as rapid moving clouds, it does not remain constant at STC value of $1000\,\mathrm{W/m^2}$ and always change. According to the existing literature, the radiation level is almost constant at time intervals less than 5 or 6 seconds, however, in this paper, we reduce the radiation change intervals from 5 s to 0.2 s to decrease the simulation time [46]. Furthermore, to show the regulation performance of the closed-loop system, we have used heavy and ideal step-type insolation changes, which are difficult to be realized by natural sunlight [47]. The numerical simulations are done in Matlab/Simulink software.

4.1. The system performance without battery and PV array distributed power management algorithm

In this study, we assume that the input radiation into the PV system at the ambient temperature $25\,^{\circ}\mathrm{C}$ to be as shown in Figure 14. It is also intended that the grid power reference signal is set to $p_{Gref} = 60\,\mathrm{kW}$. This battery-free scenario is implemented with the classic MPPT based on IC algorithm without any power curtailment ability. The MPPT voltage step is set to $\Delta V = 0.5\,\mathrm{V}$ and its sampling time is considered as 0.005 s. Therefore, corresponding to the radiation profile in Figure 14, the power delivered to the grid is illustrated in Figure 15. As it can be seen from this figure, the power delivered to the

grid deviates from the desired reference value of $p_{Gref} = 60\text{kW}$, which is not desirable. We consider the radiation profile as in Figure 14 in all subsequent scenarios.

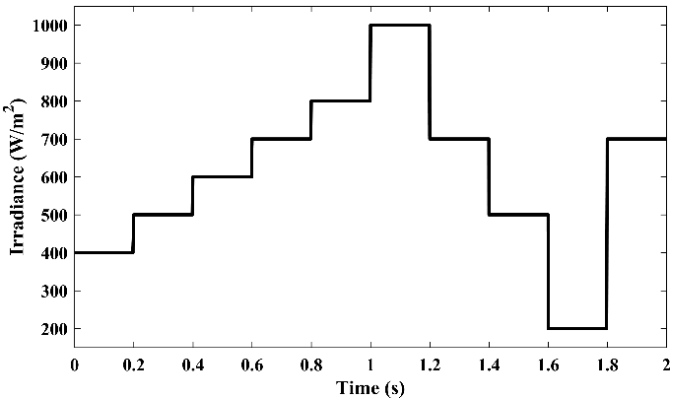

Fig. 14. The input radiation to the PV-battery system at the ambient temperature of $25\ ^{\circ}C$

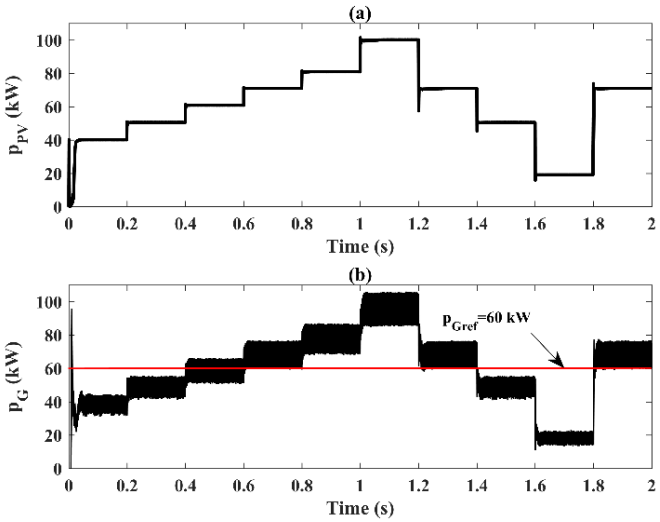

Fig. 15. The power profile with classic MPPT and without battery, (a) PV array power, (b) grid power

4.2. The system performance with battery distributed power management system and the classic MPPT

As it can be seen from Figure 15, due to the irradiation changes, the injected power to the grid is changed considerably and to solve this problem, the battery and its distributed control system is employed in this scenario. However, the battery performance depends on its charge level SOC. Based on the battery charge level and its upper and lower limits, three functional areas can be determined for the battery. Region A: $SOC > 90\%$, region B: $10\% \le SOC \le 90\%$, and region C: $SOC < 10\%$. Since one of the objectives of this paper is to emphasize the critical state in which the PV array has excess power, and the battery cannot absorb it, thus here only the region A is considered.

Assuming that the battery charge level is 95%, the power produced by the PV system p_{PV}, the power supplied to the grid p_G, and the battery power p_B are as shown in Figure 16. As can be seen from figure, at a charge level of 95%, the battery has been able to compensate completely the power shortage in time intervals of 0-0.4 s and 1.4-1.6 s. Within the interval 1.6-1.8 second a large part of the power shortage has been compensated as well. Nevertheless, when the PV array has the excess power, the battery cannot compensate this over production and in these periods, the delivered power to the grid deviates from its reference value and is not desirable.

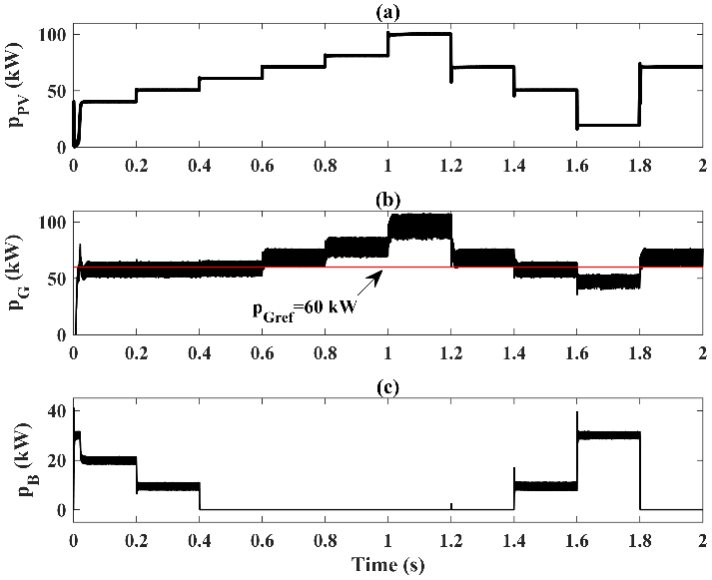

Fig. 16. The power profiles corresponding to the radiation pattern in Figure 14 with battery under $SOC = 95\%$ and classic MPPT, (a) PV array power p_{PV}, (b) supplied power to grid p_G (c) battery power p_B

4.3. The system performance with both PV and battery distributed power controllers

In this section, we want to examine the performance of the proposed decentralized power management systems in Figures 11 and 13 to supply the demanded grid power of $p_{Gref} = 60\text{kW}$ in all battery operational regions.

4.3.1 Region A: $SOC > 90\%$

In this case, in the presence of the proposed distributed algorithms for the battery and PV array in Figures 11 and 13, the PV array, grid and battery power profiles are shown in Figures 17 and 18. Figure 17 shows the control system performance corresponding to the shifting of PV array operating point to the right of the MPP with the voltage step of $\Delta V = 1\text{V}$, and Figure 18 corresponds to the change of the operating point of the PV array to the left of the MPP with the voltage step of $\Delta V = 2.5\text{V}$. According to Figure 12, during PV power curtailment, since the MPP distance from the left-side point is far than the right operating point, to improve the response speed during disturbances, the voltage step ΔV for the motion to the left operating point is taken larger than the corresponding step to move to the right operating point. Comparing Figure 16 with Figures 17 and 18, it can be found that the proposed decentralized energy management system in the time interval of 0.6-1.4 s, when the battery is full and PV array has an overproduction, has reduced the PV array power p_{PV} and made it to be equal to the grid demanded power p_G.

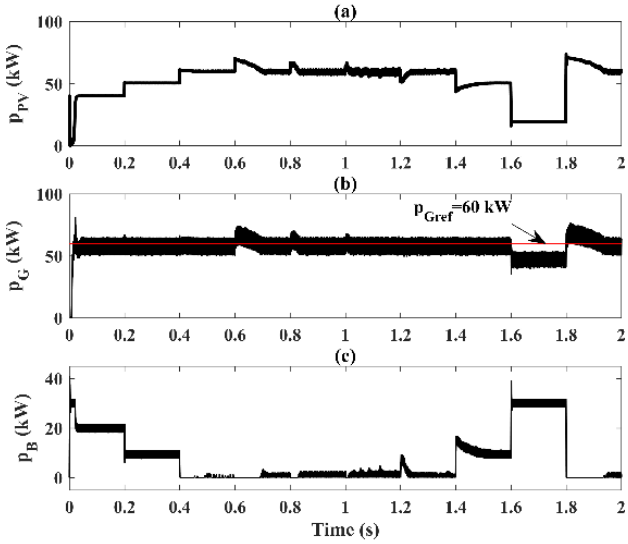

Fig. 17. The power profiles corresponding to the radiation pattern in Figure 14 with battery under $SOC = 95\%$ and proposed PV and battery distributed controllers with a motion to the right of MPP, (a) PV array power p_{PV}, (b) supplied power to grid p_G (c) battery power p_B

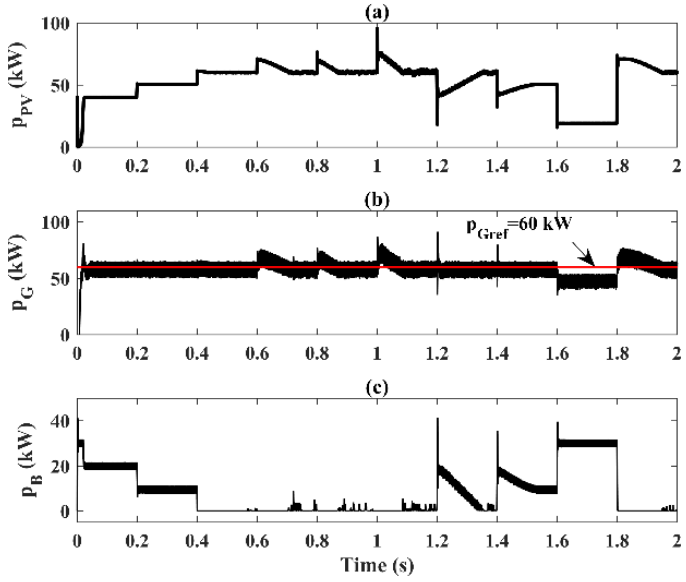

Fig. 18. The power profiles corresponding to the radiation pattern in Figure 14 with battery under $SOC = 95\%$ and proposed PV and battery distributed controllers with a motion to the left of MPP, (a) PV array power p_{PV}, (b) supplied power to grid p_G (c) battery power p_B

4.3.2 The region B: $10\% \le SOC \le 90\%$

Figures 19 and 20 show the PV array, grid and battery power profiles corresponding to $SOC = 50\%$ with the ability to deviate to the right and left of the MPP, respectively. As it can be seen from these figures, the battery can both absorb and supply the power, and as a result dynamic performance of the system is better than those of Figures 17 and 18.

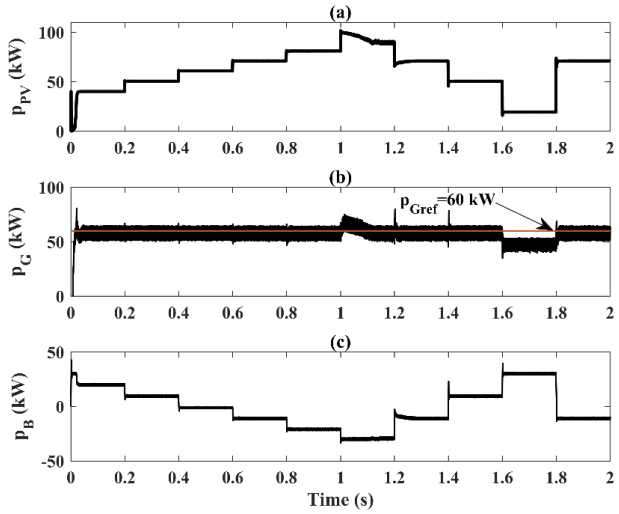

Fig. 19. The power profiles corresponding to the radiation pattern in Fig. 14 with battery under $SOC = 50\%$ and proposed PV and battery distributed controllers with a motion to the right of MPP, (a) PV array power p_{PV}, (b) supplied power to grid p_G (c) battery power p_B

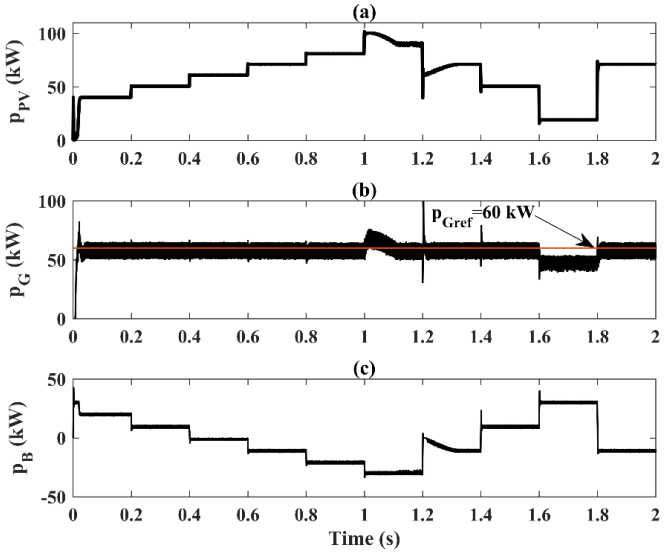

Fig. 20. The power profiles corresponding to the radiation pattern in Figure 14 with battery under $SOC = 50\%$ and proposed PV and battery distributed controllers with a motion to the left of MPP, (a) PV array power p_{PV}, (b) supplied power to grid p_G (c) battery power p_B

Figures 21, 22 and 23 illustrate the case studies including $G = 0 W/m^2$, $p_{Gref} = 0$ kW and variable p_{Gref}, respectively. As it can be seen from Figure 21, during nights that the PV power is not available the PV/battery system may not be able to provide the requested power by the network. Figure 22 and 23 show the grid following capability of the proposed power management systems over a wide range of p_{Gref} including positive, zero and negative values of this signal.

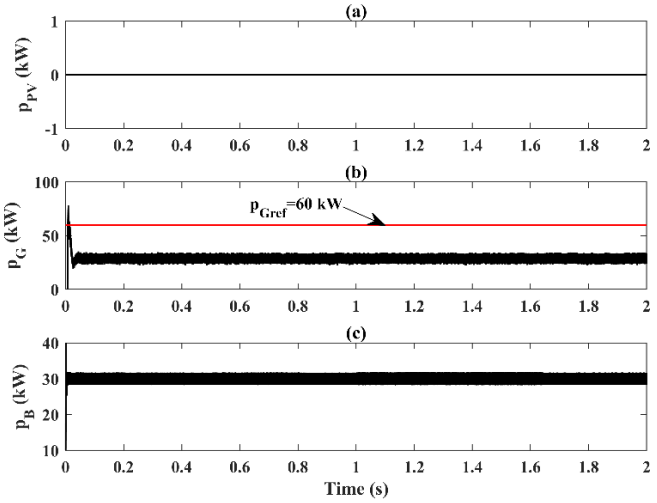

Fig. 21. The power profiles corresponding to the zero radiation $G = 0W/m^2$ with battery under $SOC = 50\%$ (a) PV array power p_{PV}, (b) supplied power to grid p_G, (c) battery power p_B

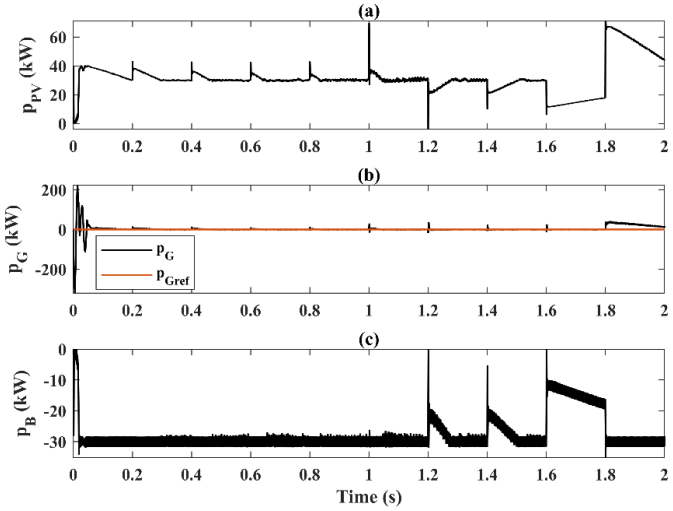

Fig. 22. The power profiles corresponding to the radiation pattern in Figure 14 with battery under $SOC = 50\%$ and $p_{Gref} = 0\,\text{kW}$, (a) PV array power p_{PV}, (b) supplied power to grid p_G (c) battery power p_B

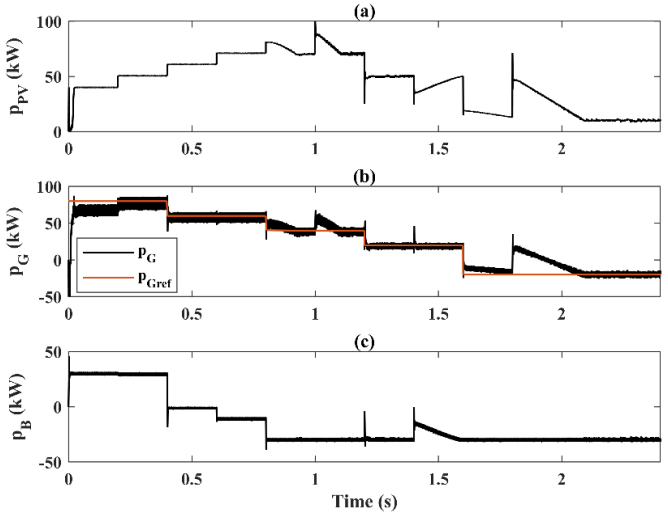

Fig. 23. The power profiles corresponding to the radiation pattern in Figure 14 with battery under $SOC = 50\%$ and variable p_{Gref}, (a) PV array power p_{PV}, (b) supplied power to grid p_G (c) battery power p_B

4.3.3 *The region C:* $SOC < 10\%$

Figures 24 and 25 show the dynamic performance of the proposed decentralized power management system for a battery charge level of $SOC = 5\%$. In this case, the battery system can only absorb energy, and therefore, the system performance has been deteriorated as compared with Figures 19 and 20 in terms of constant power generation.

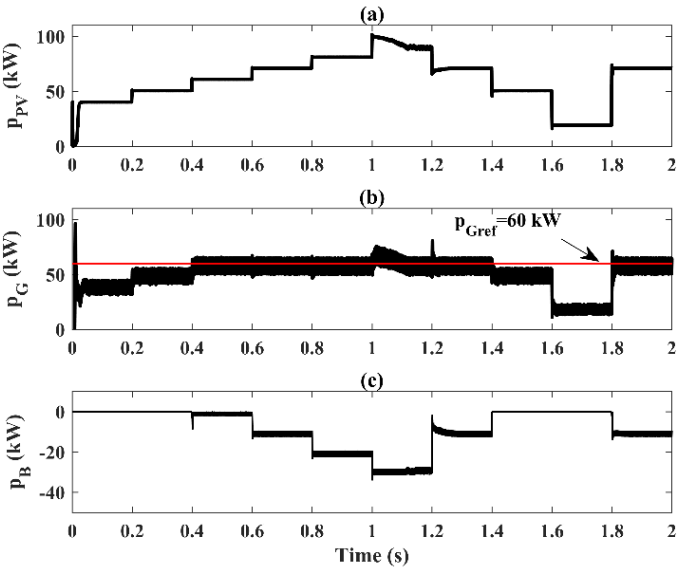

Fig. 24. The power profiles corresponding to the radiation pattern in Figure 14 with battery under $SOC = 5\%$ and proposed PV and battery distributed controllers with a motion to the right of MPP, (a) PV array power p_{PV}, (b) supplied power to grid p_G (c) battery power p_B

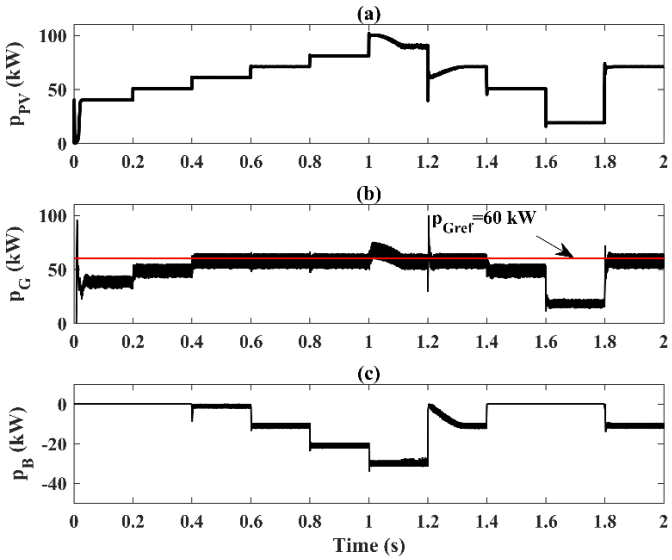

Fig. 25. The power profiles corresponding to the radiation pattern in Figure 14 with battery under $SOC = 5\%$ and proposed PV and battery distributed controllers with a motion to the left of MPP, (a) PV array power p_{PV}, (b) supplied power to grid p_G (c) battery power p_B

In all preceding case studies, one can see that there are some intervals in which the PV/battery system is not able to follow exactly the reference power demanded by the grid. According to [48], usually a hydrogen secondary backup consisting of a fuel cell and electrolyzer is considered as a long-term energy storage beside of the primary battery backup as a short-term energy storage for the renewable-energy sources. Integrating these new storage devices in the PV/battery system and extension of the proposed distributed energy management system is the topic of future research. However, the interaction of these two different types of energy storage backups on the overall lifetime and efficiency is a challenging issue. The energy management system must make the system operates in a way that the lifetime of the different elements is not deteriorated; the operation and maintenance costs are reduced, and the system efficiency is increased. Unfortunately, these objectives are in the opposite with each other [49]. For instance, as a general rule, the batteries must not be overcharged or underdischarged since as it is well-known the batteries' lifetime is dramatically decreased. In this situation, if the hydrogen equipment operation bandwidth is taken as short as possible, a more efficient system is obtained since the hydrogen path always has lower efficiency than batteries. However, the drawback is frequent battery usage and as a result their reduced lifetime [50]. On the other hand, if the bandwidth of the hydrogen equipment is increased, this solution causes a high number of start and stops of the fuel cell and electrolyzer, and consequently, reduces the lifetime of these devices to the benefit of the batteries. This is because when the FC and eloctrolyzer powers are adapted with the grid demanded power, a charge-sustaining mode for the batteries is provided increasing the batteries lifetime [48]. According to preceding discussion, the implementation of an energy management system that takes into account all the technical and economic requirements of a renewable energy system with its own backup systems is a challenging problem [48]. To perform this kind of studies, namely to investigate the influence of the energy management systems on the operational costs, lifetime and efficiency of the overall renewable energy system, the long-term simulations on the basis of simplified mathematical models are required. From the literature review it can be drawn that the papers in the area of energy management systems (EMS) of renewable energy sources can be classified into two large groups depending on the objectives of the EMS and type of studies at hand.

In the first group, the short-term dynamical performance of the closed-loop system during variable climatic conditions and demanded power variations is of interest. References [8]-[38] are relevant examples of this kind of studies. The simulations carried out in this kind of works are based on the detailed mathematical models of different components within the system. The simulation step time is very small and the length of time in which the simulations are made is of an order of several seconds, which is enough to study the dynamics of the closed-loop control system during disturbances. The present work belongs to this category of studies.

On the other hand, there are many articles whose main objectives are to study the system behavior during long periods of time (months, years or the whole life of the system) with a simulation step of one hour. Of these works we can mention [51-60]. In these papers, the dynamic behaviors of the energy sources are neglected and simplified and static models of each component are used. The controls of renewable-energy resources (PV panels and wind turbines) are considered to be independent of EMS. Only the power generated by the PV and wind turbines should be known every hour. The focus of these works is on the evaluation of the performance parameters such as efficiency, cost, lifetime, complexity, sizing, etc. Obviously the current work can be extended as a future work considering suitable lifetime, economic and efficiency models proposed in this area of research and compared with other energy management strategies in a long-term study.

5. Conclusion

PV arrays, due to their fluctuating output power, cause undesirable effects from stability and power quality point of views on the network they are connected to. One of the efficient ways to reduce the PV power fluctuations and provide a controllable constant power profile is to use energy storage systems such as batteries. To reach these objectives, this paper presents a distributed power management controller for the battery and PV arrays with the ability of PV power curtailment. Unlike to the conventional centralized power controllers, the proposed supervisory control system has a distributed structure with some advantages such as simplicity, high reliability, no need for switching between local controllers, and the ability to integrate new units into the system without making any major changes to the control system structure and its settings. The simulation results in a wide range of operating points and different battery conditions, such as fully charged and fully discharged conditions, represent the satisfactory dynamical performance of the proposed distributed power management system in terms of supplying constant power demanded by the grid.

References

[1] Technology roadmap solar photovoltaic energy, *International Energy Agency*, October 2010, available from: https://www.iea.org/publications/freepublications/publication/pv_roadmap.pdf

[2] Kouro, S., J. I. Leon, D. Vinnikov and L. G. Franquelo, "Grid-connected photovoltaic systems: an overview of recent research and emerging PV converter technology." *IEEE Industrial Electronics Magazine* 9, no. 1 (2015): 47-61.

[3] Liu, X., A. Aichhorn, L. Liu and H. Li, "Coordinated control of distributed energy storage system with tap changer transformers for voltage rise mitigation under high photovoltaic penetration." *IEEE Transactions on Smart Grid* 3, no. 2 (2012): 897-906.

[4] Hill, C. A., M. C. Such, D. Chen, J. Gonzalez and W. M. Grady, "Battery energy storage for enabling integration of distributed solar power generation." in *IEEE Transactions on Smart Grid* 3, no. 2 (2012): 850-857.

[5] Shivashankar, S., S. Mekhilef, H. Mokhlis, and M. Karimi, "Mitigating methods of power fluctuation of photovoltaic (PV)

sources–a review." *Renewable and Sustainable Energy Reviews* 59, (2016): 1170-1184.
[6] Yi, Z., W. Dong and A. H. Etemadi, "A Unified control and power management scheme for PV-battery-based hybrid microgrids for both grid-connected and islanded modes." *IEEE Transactions on Smart Grid 9*, no. 6 (2018): 5975-5985.
[7] Alam, M. J. E., K. M. Muttaqi and D. Sutanto, "A novel approach for ramp-rate control of solar PV using energy storage to mitigate output fluctuations caused by cloud passing." *IEEE Transactions on Energy Conversion* 29, no. 2 (2014): 507-518.
[8] Lazzari, R., C. Parma, A. De Marco & S. Bittanti, "Enabling a flexible exchange of energy of a photovoltaic plant with the grid by means of a controlled storage system." *International Journal of Control* 88, no. 7 (2015): 1353-1365.
[9] Simões, M. G., T. D. C. Busarello, A. S. Bubshait, F. Harirchi, J. A. Pomilio and F. Blaabjerg, "Interactive smart battery storage for a PV and wind hybrid energy management control based on conservative power theory." *International Journal of Control* 89, no. 4 (2016): 850-870.
[10] Eghtedarpour, N., E. Farjah, "Control strategy for distributed integration of photovoltaic and energy storage systems in DC micro-grids." *Renewable Energy* 45, (2012): 96-110.
[11] Schonbergerschonberger, J., R. Duke and S. D. Round, "DC-bus signaling: a distributed control strategy for a hybrid renewable nanogrid." *IEEE Transactions on Industrial Electronics* 53, no. 5 (2006): 1453-1460.
[12] Omran, W. A., M. Kazerani and M. M. A. Salama, "Investigation of methods for reduction of power fluctuations generated from large grid-connected photovoltaic systems." *IEEE Transactions on Energy Conversion* 26, no. 1 (2011): 318-327.
[13] Kim, S., J. Jeon, C. Cho, J. Ahn and S. Kwon, "Dynamic modeling and control of a grid-connected hybrid generation system with versatile power transfer." *IEEE Transactions on Industrial Electronics* 55, no. 4 (2008): 1677-1688.
[14] Tani, A., M. B. Camara and B. Dakyo, "Energy management in the decentralized generation systems based on renewable energy—ultracapacitors and battery to compensate the wind/load power fluctuations," *IEEE Transactions on Industry Applications* 51, no. 2 (2015): 1817-1827.
[15] Adhikari, S., and F. Li, "Coordinated V-f and P-Q control of solar photovoltaic generators with MPPT and battery storage in microgrids," *IEEE Transactions on Smart Grid* 5, no. 3 (2014): 1270-1281.
[16] Wang, T., H. Kamath and S. Willard, "Control and optimization of grid-tied photovoltaic storage systems using model predictive control." *IEEE Transactions on Smart Grid* 5, no. 2 (2014): 1010-1017.
[17] Kim, S., S. Bae, Y. C. Kang and J. Park, "Energy management based on the photovoltaic HPCS with an energy storage device." *IEEE Transactions on Industrial Electronics* 62, no. 7 (2015): 4608-4617.
[18] Daud, M. Z., Azah Mohamed, M.A. Hannan, "An improved control method of battery energy storage system for hourly dispatch of photovoltaic power sources." *Energy Conversion and Management* 73, (2013): 256-270.
[19] Li, X., D. Hui and X. Lai, "Battery energy storage station (BESS)-based smoothing control of photovoltaic (PV) and wind power generation fluctuations." *IEEE Transactions on Sustainable Energy* 4, no. 2 (2013): 464-473.
[20] Koohi-Kamali, S., N.A. Rahim, H. Mokhlis, "Smart power management algorithm in microgrid consisting of photovoltaic, diesel, and battery storage plants considering variations in sunlight, temperature, and load." *Energy Conversion and Management* 84, (2014): 562-582.
[21] Teleke, S., M. E. Baran, S. Bhattacharya and A. Q. Huang, "Rule-based control of battery energy storage for dispatching intermittent renewable sources." in *IEEE Transactions on Sustainable Energy* 1, no. 3 (2010): 117-124.
[22] Lamsal, D., V. Sreeram, Y. Mishra and D. Kumar, "Achieving a minimum power fluctuation rate in wind and photovoltaic output power using discrete Kalman filter based on weighted average approach." *IET Renewable Power Generation* 12, no. 6 (2018): 633-638.
[23] Kewat, S., B. Singh and I. Hussain, "Power management in PV-battery-hydro based standalone microgrid." *IET Renewable Power Generation* 12, no. 4 (2018): 391-398.
[24] Eghtedarpour, N., and E. Farjah, "Distributed charge/discharge control of energy storages in a renewable-energy-based DC micro-grid." *IET Renewable Power Generation* 8, no. 1 (2014): 45-57.
[25] Wang, G., M. Ciobotaru, and V. G. Agelidis, "Power smoothing of large solar PV plant using hybrid energy storage." *IEEE Transactions on Sustainable Energy* 5, no. 3 (2014): 834-842.
[26] Wang, G., M. Ciobotaru and V. G. Agelidis, "Power management for improved dispatch of utility-scale PV plants." *IEEE Transactions on Power Systems* 31, no. 3 (2016): 2297-2306.
[27] Datta, M., T. Senjyu, A. Yona, and T. Funabashi, "Photovoltaic output power fluctuations smoothing by selecting optimal capacity of battery for a photovoltaic-diesel hybrid system." *Electric Power Components and Systems* 39, no. 7 (2011): 621-644.
[28] Lu, D., H. Fakham, T. Zhou, B. François, "Application of Petri nets for the energy management of a photovoltaic based power station including storage units." *Renewable Energy* 35, no. 6 (2010): 1117-1124.
[29] Sukumar, S., H. Mokhlis, S. Mekhilef, M. Karimi, and S. Raza, "Ramp-rate control approach based on dynamic smoothing parameter to mitigate solar PV output fluctuations." *International Journal of Electrical Power & Energy Systems* 96, (2018): 296-305.
[30] Choudar, A., D. Boukhetala, S. Barkat, J-M Brucker, "A local energy management of a hybrid PV-storage based distributed generation for microgrids." *Energy Conversion and Management* 90, (2015): 21-33.
[31] Tafti, H. D., A. I. Maswood, G. Konstantinou, J. Pou and F. Blaabjerg, "A general constant power generation algorithm for photovoltaic systems." *IEEE Transactions on Power Electronics* 33, no. 5 (2018): 4088-4101.
[32] Sangwongwanich, A., Y. Yang and F. Blaabjerg, "High-performance constant power generation in grid-connected PV systems." *IEEE Transactions on Power Electronics* 31, no. 3 (2016): 1822-1825.
[33] Sangwongwanich, A., Y. Yang, F. Blaabjerg and H. Wang, "Benchmarking of constant power generation strategies for single-phase grid-connected photovoltaic systems." *IEEE Transactions on Industry Applications*, vol. 54, no. 1 (2018): 447-457.
[34] Sangwongwanich, A., Y. Yang and F. Blaabjerg, "A sensorless power reserve control strategy for two-stage grid-connected PV systems." *IEEE Transactions on Power Electronics* 32, no. 11 (2017): 8559-8569.
[35] Miñambres-Marcos, V. M., M. Á. Guerrero-Martínez, F. Barrero-González, and M. I. Milanés-Montero, "A grid connected photovoltaic inverter with battery-supercapacitor hybrid energy storage." *Sensors* 17, no. 8 (2017): 1-18.
[36] Mousazadeh Mousavi, SY, A. Jalilian, M. Savaghebi, J. M. Guerrero, "Power quality enhancement and power management of a multifunctional interfacing inverter for PV and battery energy storage system." *International Transactions on Electrical Energy Systems 28*, no. 12 (2018): 1-15.
[37] Aly, M. M., E. Abdelkarim, and M. Abdel-Akher, "Mitigation of photovoltaic power generation fluctuations using plug-in hybrid electric vehicles storage batteries." *International Transactions on Electrical Energy Systems* 25, no. 12 (2015): 3720-3737.

[38] Wu, H., S. Wang, B. Zhao, C. Zhu, "Energy management and control strategy of a grid-connected PV/battery system." *International Transactions on Electrical Energy Systems* 25, no. 8 (2014): 1590-1602.
[39] Hejri, M., H. Mokhtari, S. Karimi, and M. Azizian, "Stability and performance analysis of a single-stage grid-connected photovoltaic system using describing function theory." *International Transactions on Electrical Energy Systems* 26, no. 9 (2016): 1898–1916.
[40] Mattei, M., G. Notton, C. Cristofari, M. Muselli, P. Poggi, "Calculation of the polycrystalline PV module temperature using a simple method of energy balance." *Renewable Energy* 31, no. 4 (2006): 553-567.
[41] Hejri, M., and H. Mokhtari, "On the Comprehensive Parametrization of the photovoltaic (PV) Cells and Modules." *IEEE Journal of Photovoltaics* 7, no. 1 (2017): 250-258.
[42] Erickson, R., and D. Maksimovic, *Fundamentals of power electronics*, second edition, 2001, Springer Science.
[43] Chen, M., and G. A. Rincon-Mora, "Accurate electrical battery model capable of predicting runtime and I-V performance." *IEEE Transactions on Energy Conversion* 21, no. 2 (2016): 504-511.
[44] Polymer Lithium Ion Battery 850-mAh TCL PL-383562 datasheet, Nov. 2003, available from: https://www.batteryspace.com/prod-specs/PL383562.pdf
[45] Olivares, D. E., *et al*., "Trends in microgrid control," *IEEE Transactions on Smart Grid* 5, no. 4 (2014): 1905-1919.
[46] Sanjeev, P., N. P. Padhy and P. Agarwal, "Peak energy management using renewable integrated DC microgrid." *IEEE Transactions on Smart Grid* 9, no. 5 (2018): 4906-4917.
[47] Xiao, W., W. G. Dunford, P. R. Palmer and A. Capel, "Regulation of photovoltaic voltage." *IEEE Transactions on Industrial Electronics* 54, no. 3 (2017): 1365-1374.
[48] Vivas, F. J., A. D. L. Heras, F. Segura and J. M. Andujar, "A review of energy management strategies for renewable hybrid energy systems with hydrogen backup." *Renewable and Sustainable Energy Reviews* 82, (2018): 126-155.
[49] Garcia-Trivino, P., L. M. Fernandez-Ramirez, A. J. Gil-Mena, F. Llorens-Iborra, C. A. Garcia-Vazquez and F. Jurado, "Optimized operation combining costs, efficiency and lifetime of hybrid renewable energy system with energy storage by battery and hydrogen in grid-connected applications." *International Journal of Hydrogen Energy* 41, (2016): 23132-23144.
[50] Varverde, L., F. J. Pino, J. Guerra, F. Rosa, "Definition, analysis and experimental investigation of operation modes in hydrogen-renewable-based power plants incorporating hybrid energy storage." *Energy Conversion and Management* 113, (2016): 290-311.
[51] Song, Z., H. Hofmann, J. Li., J. Hou, X. Han and M. Ouyang, "Energy management strategies comparison for electric vehicles with hybrid energy storage system." *Applied Energy* 134, (2014): 321-331.
[52] Varverde, L., F. J. Pino, J. Guerra, F. Rosa, "Definition, analysis and experimental investigation of operation modes in hydrogen-renewable-based power plants incorporating hybrid energy storage," *Energy Conversion and Management* 113, (2016): 290-311.
[53] Torreglosa, J. P., P. Garcia, L. M. Fernandez and F. Jurado, "Hierarchical energy management system for stand-alone hybrid system based on generation costs and cascade control." *Energy Conversion and Management* 77, (2014): 514-526.
[54] Torreglosa, J. P., P. Garcia, L. M. Fernandez and F. Jurado, "Energy dispatching based on predictive controller of an off-grid wind turbine/photovoltaic/hydrogen/battery hybrid system." *Renewable Energy* 74, (2015): 326-336.
[55] Garcia, P., J. P. Torreglosa, L. M. Fernandez and F. Jurado, "Optimal energy management system for stand-alone winf turbine/photovoltaic/hydrogen/battery hybrid system with supervisory control based on fuzzy logic." *International Journal of Hydrogen Energy* 38, (2013): 14146-14158.
[56] Cozzolino, R., L. Tribioli, G. Bella, "Power management of a hybrid renewable system for artificial islands: a case study." *Energy* 106, (2016): 774-789.
[57] Torreglosa, J. P., P. Garcia-Trivino and L. M. Fernandez-Ramirez, "Control based on techno-economic optimization of renewable hybrid energy system for stand-alone applications." *Expert Systems with Applications* 51, (2016): 59-75.
[58] Garcia-Trivino, P., L. M. Fernandez-Ramirez, A. J. Gil-Mena, F. Llorens-Iborra, C. A. Garcia-Vazquez and F. Jurado, "Optimized operation combining costs, efficiency and lifetime of hybrid renewable energy system with energy storage by battery and hydrogen in grid-connected applications." *International Journal of Hydrogen Energy* 41, (2016): 23132-23144.
[59] Garcia, P., C. A. Garcia, L. M. Fernandez, F. Llorens and F. Jurado, "ANFIS-based control of a grid-connected hybrid system integrating renewable energies, hydrogen and batteries." *IEEE Transactions on Industrial Informatics* 10, no. 2 (2014): 1107-1117.
[60] Bruni, G., S. Cordiner and V. Mulone, "Domestic distributed power generation: effect of sizing and energy management strategy on the environmental efficiency of a photovoltaic-battery-fuel cell system," *Energy* 77, (2014): 133-143.